Self- and Cross-Phase-Modulation Coefficients in KDP Crystals Measured by a *Z*-Scan Technique

In the interaction of strong fields with matter, considerable interest has been shown in the development of high-efficiency frequency up-conversion of ultrashort laser pulses. One important area of interest is in ultrafast laser–solid interactions where up-conversion can lead to higher absorption due to higher-density interactions[1] and to an enhancement of the pulse-intensity contrast by many orders of magnitude, allowing the high-intensity pulse to interact with the solid-density material.[2] Efficient second-harmonic generation in KDP has been reported for ultrafast laser beams at intensities up to 400 GW/cm^2.[3] In this intensity region, nonlinear effects such as self- and cross-phase modulation[4,5] (SPM, XPM) originating from third-order nonlinear susceptibility $\chi^{(3)}$ may limit the efficiency of ultra-intense frequency-conversion processes that involve co-propagation of two beams with different wavelengths. SPM and XPM are responsible for spectral broadening in optical fibers and have been used in pulse compression to produce ultrashort laser pulses.[6] XPM has been observed in fiber Raman soliton lasers[7,8] and has proven to be important in optical parametric oscillators, optical parametric amplifiers,[9] and the harmonic-generation process in bulk nonlinear crystals.[10,11] Nonlinear phase changes can destroy the phase coherence required for efficient conversion. *Z*-scan,[12,13] four-wave mixing,[14,15] ellipse rotation,[16] and nonlinear interferometer[17,18] techniques have been used to measure the nonlinear refractive index $n_2\left[n_2 = 3/8n\chi^{(3)}\right]$ associated with SPM. Nonlinear refractive index coefficients associated with SPM in KDP crystals, which are widely used in frequency conversion,[19,3] were measured by degenerate three-wave mixing[20] and time-resolved interferomery[21] at 1 μm. In this article we report on the results of the single-beam *Z*-scan measurement[12,13] of the nonlinear refractive index associated with SPM at wavelengths of 1.053 μm, 0.527 μm, and 0.351 μm and two-color *Z*-scan[22] to measure the nonlinear coefficients of XPM between 1.053 μm and 0.527 μm in a KDP crystal. In the two-color *Z*-scan measurement, two collinear beams with different wavelengths are used; a weak probe beam can be defocused by the action of the strong pump beam in a thin sample.[22] The far-field intensity variation is used to determine the optical nonlinearity from XPM as the sample is moved along the propagation direction (z axis) of the focused beams.

A schematic of the setup is shown in Fig. 74.61. Infrared (IR) laser pulses (λ_1 = 1.053 μm), second-harmonic (SH) pulses (λ_2 = 0.527 μm), or third-harmonic (TH) pulses (λ_3 = 0.351 μm) are transmitted through an aperture A1 and can be treated as top-hat beams. Second-harmonic pulses are generated using a KDP type-I crystal, and third-harmonic pulses are generated using two KDP type-II crystals.[23] We use the top-hat spatial profile because it increases the measurement sensitivity.[24] This top-hat beam then co-propagates through a lens with focal length f_1 for IR, f_2 for SH, and f_3 for TH. The focal lengths f_1, f_2, and f_3 are slightly different due to the dispersion of the lens. The electric-field distribution near the focal point $E_i(r,z,t)$ (i = 1,2,3) is described by Lommel functions.[25] It has an Airy radius at the focal spot of 1.22 $\lambda_i F_i$, where $F_i = f_i/2a$ and $2a$ is the diameter of aperture A1. The beam waist (w_{0i}) is defined as $w_{0i} = \lambda_i F_i$. The Rayleigh range (z_{0i}) is $\pi w_{0i}^2/\lambda_i$. A nonlinear crystal located in the focal region will introduce phase modulation proportional to the intensity. The single-beam *Z*-scan is performed when only one wavelength beam passes through A1. In these cases, if the sample thickness is much less than the Rayleigh range z_{0i} and the nonlinear absorption can be ignored, the field distribution at the exit surface of the sample can be expressed simply by

$$E_{ei}(r,z,t) = E_i(r,z,t)\,\exp\left\{ik_i L_{\mathrm{eff}_i}\left[\gamma_i\left|E_i(r,z,t)\right|^2\right]\right\}, \quad i = 1,2,3 \tag{1}$$

where $k_i = 2\pi/\lambda_i$, $L_{\mathrm{eff}_i} = \left[1-\exp(-\alpha_i L)\right]/\alpha_i$ is the effective sample thickness, α_i is the linear absorption coefficient, and γ_i is the nonlinear refraction coefficient, which is related to n_{2i} by $n_{2i} = \left(cn_0/40\pi\right)\gamma_i\left(m^2/\mathrm{W}\right)$, where c(m/s) is the speed of light in vacuum and n_0 is the linear index of refraction. The incident electric field $E_i(r,z,t)$ is normalized so that $I_i = \left|E_i(r,z,t)\right|^2$.

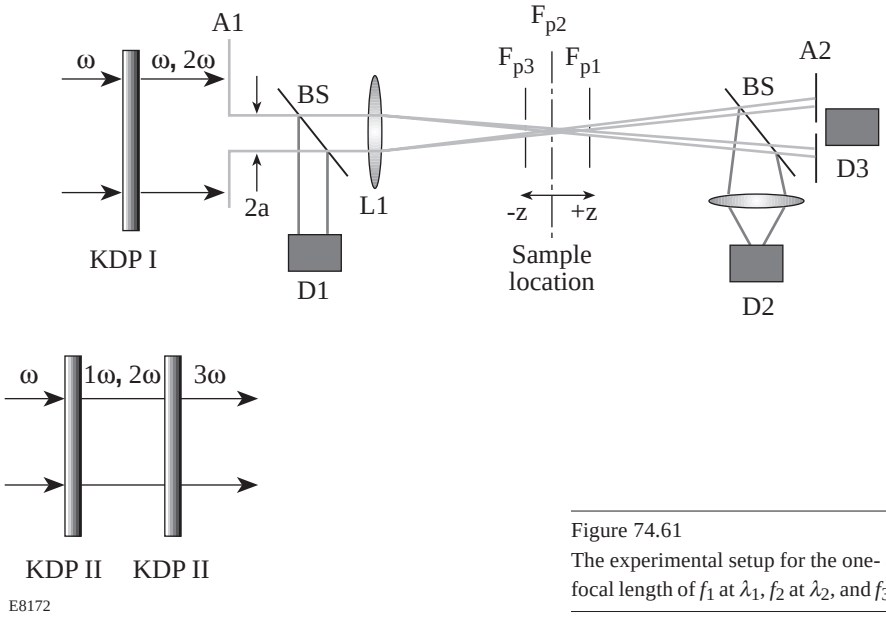

Figure 74.61
The experimental setup for the one- and two-beam *Z*-scans. A1, A2: aperture; L1: lens with focal length of f_1 at λ_1, f_2 at λ_2, and f_3 at λ_3; D1, D2, D3: photon detectors; BS: beam splitter.

In the two-color *Z*-scan, we measured the cross-phase-modulation coefficients between optical waves at λ_1 and λ_2. The output unconverted IR (pump beam) and SH pulses (probe beam) from a frequency doubler co-propagate through A1 (Fig. 74.61). The field distribution at the exit surface of the sample is

$$E_{e1}(r,z,t) = E_1(r,z,t) \exp\left\{ik_1 L_{\text{eff}_1}\left[\gamma_1 |E_1(r,z,t)|^2 + 2\gamma_{21}|E_2(r,z,t+\tau)|^2\right]\right\}, \quad (2)$$

$$E_{e2}(r,z,t+\tau) = E_2(r,z,t+\tau) \exp\left\{ik_2 L_{\text{eff}_2}\left[\gamma_2 |E_2(r,z,t+\tau)|^2 + 2\gamma_{12}|E_1(r,z,t)|^2\right]\right\}, \quad (3)$$

where τ is the time delay between IR and SH pulses introduced in the KDP type-I frequency-doubling crystal. In the exponent of Eqs. (2) and (3), the first term reflects the impact of self-phase modulation, and the second term reflects the phase modulation induced by an optical wave of the other wavelength. If the optical wave intensity at wavelength λ_2 is weak enough that $\gamma_2|E_2|^2 << \pi$, the second term in the exponential of Eq. (2) and first term in Eq. (3) can be ignored. Therefore, as the nonlinear crystal is moved along the z axis, the transmittance of the electric field at wavelength λ_1 through a finite aperture in the far field is determined by the self-phase modulation of the λ_1 optical wave, while the transmittance of the electric field at wavelength λ_2 is determined by the cross-phase modulation due to the λ_1 optical wave.

When the Fresnel number $w_{0i}/\lambda_i D$ is much smaller than unity, where D is the distance from sample to the aperture A2, the field distribution $E_{\text{A2}}(\rho,z,t)$ at the sampling aperture A2 (Fig. 74.61) is proportional to the Fourier transform of field at the exit surface of the sample.[26] The normalized *Z*-scan power transmittance is

$$T(z) = \frac{\int_{-\infty}^{\infty}\int_0^{r_a} \left|E_{\text{A2}}(\rho,z,t)\right|^2 \rho d\rho dt}{\int_{-\infty}^{\infty}\int_0^{r_a} \left|E_{i_{\text{A2}}}(\rho,z,t)\right|^2 \rho d\rho dt}, \quad (4)$$

where r_a is the radius of aperture A2 and $E_{i\text{A2}}$ is the electric field at A2 without nonlinear crystal. Equation (4) gives the *Z*-scan fluence transmittance $T(z)$ as a function of crystal position.

Figure 74.62 shows numerical examples of the normalized transmittance as a function of sample positions in the presence of SPM and XPM, respectively. For all of the curves the on-axis nonlinear phase accumulation (either self- or cross-phase) is chosen to be $\Phi_0 = 0.4$, where $\Phi_0 = k_i L_{\text{eff}_i}\gamma_i I_0$ and I_0 is the on-axis peak intensity. The curves compare the effects of self- and cross-phase modulation on the transmittance of the two beams through the aperture. Even though the phase shifts are the same, the different focusing of the two beams means that transmittance as a function of crystal position will differ for the

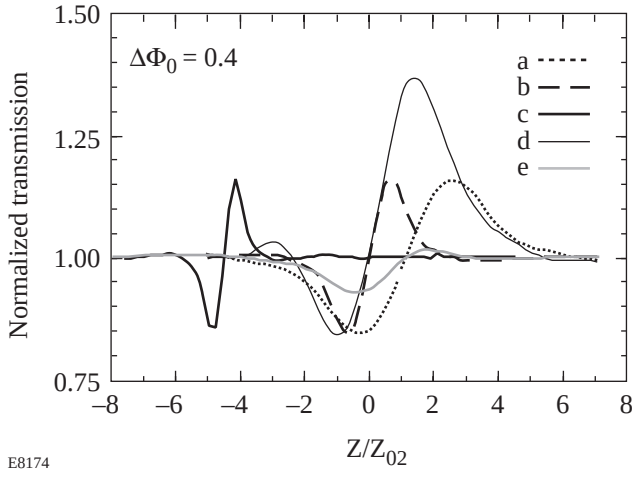

Figure 74.62
The effect of SPM and XPM on transmitting the beams at different wavelengths through the aperture (A2 in Fig. 74.61). In all cases, the nonlinear phase shift is $\Phi_0 = 0.4$. Curves (a), (b), and (c) are the transmittance of the single-color *Z*-scan at wavelengths of $\lambda_1 = 1053$ nm, $\lambda_2 = 527$ nm, and $\lambda_3 = 351$ nm. Curve (d) is the transmittance of the two-color (λ_1,λ_2) *Z*-scan with a strong λ_1 and weak λ_2. Curve (e) is the transmittance of the two-color (λ_1,λ_2) *Z*-scan for a strong λ_2 and λ_1. z/z_{02} is the position in terms of the Rayleigh range of the second-harmonic beam.

different physical processes. This can be beneficial in distinguishing the different effects, in particular, eliminating the contamination of SPM in the XPM measurements.

Curves (a), (b) and (c) in Fig. 74.62 show the effects of self-phase modulation on the transmittance for the beam at wavelengths of 1.053 μm (λ_1), 0.527 μm (λ_2), and 0.351 μm (λ_3), respectively. Since the *f* number of the system at λ_1 and λ_2 is about the same, the Rayleigh range z_{01} is twice z_{02}. The distance between peak and valley corresponding to the λ_2 optical wave is half that of the λ_1 optical wave. Curve (d) shows the effects of XPM of λ_1 on the transmittance of the weak λ_2 beam $\left(\lambda_2 = \lambda_1/2\right)$. The asymmetry in the relative decrease or increase in transmittance is mainly due to the dispersion of the focusing lens. The focal length is slightly longer for the λ_1 optical wave. The irradiance of electric field at 1.053 μm induces a positive lens for the λ_2 wave in the thin sample near its focus since $n_{21} > 0$. With the sample on the $-z$ side of the λ_1 focus (Fig. 74.61), the positive lensing effect tends to augment diffraction; therefore, the aperture transmittance is reduced. When the sample moves on the $+z$ side of the λ_1 focus, the positive lensing effect tends to collimate the beam and increase the transmittance through the aperture. The transmittance reaches a maximum when the sample is located approximately at the focal point of λ_1 (i.e, F_{p1} in Fig. 74.61) because the maximum intensity-dependent phase distortion takes place at F_{p1}. Curve (e) shows the effects of XPM of λ_2 on the transmittance of a weak λ_1 beam, which is opposite to curve (d). The asymmetry in the relative decrease or increase in transmittance is similar to curve (d) but the sensitivity is much smaller in this case. Because the pump beam's spot diameter is half that of the probe beam, only the center portion of the probe beam will experience nonlinear phase distortion.

In the experiment, 2.0-ps, 1-μm laser pulses are generated from a chirped-pulse-amplification laser system.[27] These 3-cm-diam pulses are incident on a 1-cm-thick, type-I KDP frequency-doubling crystal for cases where n_2 at 0.527 μm and a XPM coefficient between 1.052 μm and 0.527 μm were measured. These pulses are incident on two 1.6-cm-thick, type-II KDP crystals to generate TH when n_2 at 0.351 μm was measured. A half-wave plate placed before the doubler tunes the polarization of the IR to control the amount of SH or TH wave generated. A BG18 filter after doubler and UG11 filter after tripler were used respectively to block light at other wavelengths.[28] A 6.8-mm-diam aperture (A1 in Fig. 74.61) is placed after the crystal to select a small portion of the IR, SH, or TH waves. The spatial profile of the pulse passing through the aperture can be regarded as a top-hat pulse. The focal lengths of the lens after the A1 aperture were determined by a far-field spot-size scan using a CCD[29] camera. The measured focal lengths are $f_1 = 76.5 \pm 0.5$ cm at $\lambda_1 = 1.053$ μm, $f_2 = 74.3 \pm 0.5$ cm at $\lambda_2 = 0.527$ μm, and $f_3 = 65.4 \pm 0.5$ cm at $\lambda_3 = 0.351$ μm. The resulting beam waists (w_{01}, w_{02}, and w_{03}) were 118 μm, 58 μm, and 34 μm, respectively. The Rayleigh ranges (z_{01}, z_{02}, and z_{03}) were 4.2 cm, 2.0 cm, and 1.0 cm. For crystals with small n_2, a longer crystal is preferred as long as the thickness is less than one-third of the corresponding Rayleigh range. In all cases, the intensity is kept well below the damage threshold. Samples with different thicknesses and cuts were used for different wavelengths. The crystals were mounted on a translation stage. To simplify the experiment analysis, a 7.5-mm-thick KDP sample cut at 90° to the wave-propagation direction was used for measuring XPM coefficients to avoid generating additional second- and third-harmonic generation during the interaction. For other axis orientations, the **k**-vector spread due to focusing would allow part of the beam to satisfy the second- or third-harmonic phase-matching condition. The transmittance through the aperture would then be due to the combined effects from refractive index changes, second-, and third-harmonic generation.

The beam splitter after the aperture (A1 in Fig. 74.61) sends a small portion of the beam to a PIN diode[30] (D1 in Fig. 74.61),

which is used to monitor the top-hat IR energy. Part of the probe beam is reflected by the beam splitter before the analyzing aperture (A2 in Fig. 74.61) to a PIN diode (D2 in Fig. 74.61) and gives the open-aperture *Z*-scan curve. From the open-aperture scan the nonlinear absorption is measured. The change of transmission due purely to the nonlinear index of refraction is determined by dividing the closed-aperture transmittance by the one without the aperture. This has the advantage of compensating for the energy fluctuations during the experiment. The linear transmittance of aperture A2, defined as the ratio of power transmitted through A2 to the total power incident on the plane of the aperture, is 0.03. The incident IR temporal full width at half-maximum (τ_{FWHM}) was 2.0±0.2 ps as measured by a single-shot autocorrelator. The SH and TH pulse widths were calculated to be 1.41 ps and 1.45 ps, respectively, in the small-signal-gain region. The energy ε of the incident IR pulse was measured by an energy meter.[31] For a Gaussian temporal profile, the on-axis peak intensity I_0 within the sample is $I_0 = \sqrt{\pi \ln 2}\varepsilon / 2w_0^2 t_{FWHM}$.[32]

Figure 74.63 shows typical *Z*-scan results obtained to determine the SPM and XPM coefficients of KDP crystals. The parameters for each case are listed in Table 74.II. The peak-to-valley configuration of all these *Z*-scans indicates a positive nonlinearity. The solid line in each of the figures is the least squares fit to the experiment data using Eq. (3) to determine the total phase accumulation Φ_0. We use a temporal separation induced in the frequency-doubling crystal (KDP I), $\tau = 0.73$ ps in Eq. (2) in the case of XPM based on the predicted temporal walk-off between pulses at different wavelengths.[33] The extraordinary IR wave moves 0.73 ps ahead of the extraordinary SH wave at the exit of the 1-cm, KDP type-I doubler.

The nonlinear coefficient γ_2 can then be calculated from $\Phi_0 = kL_{eff}\gamma_{12}I_0$. There are several error sources in the measurement: the error in the curve fit, in measuring the crystal thickness, and in measuring the pulse width and energy that determine beam intensity. The least squares fit for the experiment data yields an error of 5%. The error for the crystal

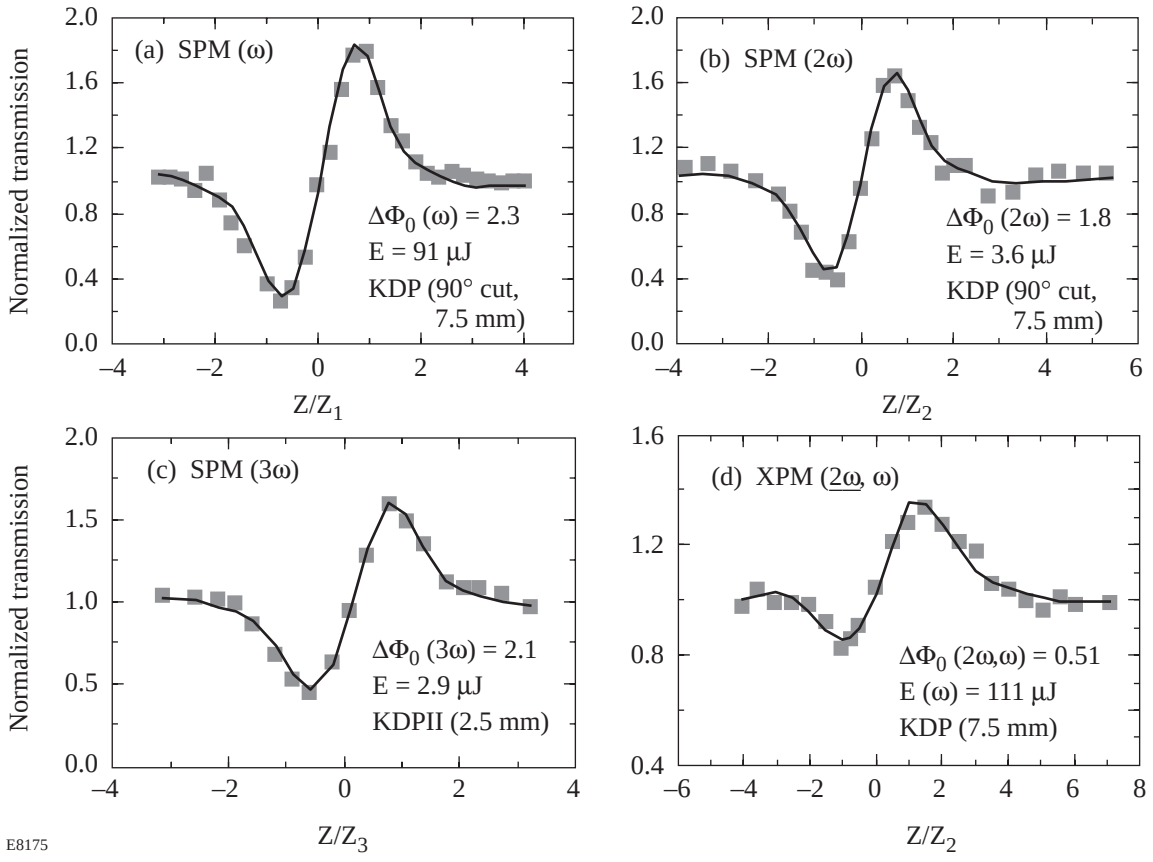

Figure 74.63
Experimental one- and two-beam *Z*-scans as a function of z/z_{0i}, $i = 1,2,3$. In all cases, the solid line is fit to determine the peak phase shift Φ_0. (a) Single beam, $\lambda_1 = 1.053$ μm, $\Phi_0 = 2.3$; (b) single beam, $\lambda_2 = 0.527$ μm, $\Phi_0 = 1.8$; (c) single beam, $\lambda_1 = 0.351$ μm, $\Phi_0 = 2.1$; and (d) two-color (λ_1,λ_2) beams, $\Phi_0 = 0.51$.

thickness is 1%. The errors for the beam waist coming from the measurement of focal length and diameter of the aperture are 1.6%. The largest error comes from measuring the IR pulse width and beam energy. The pulse widths of SH and TH were calculated based on the measurement of the IR pulse. The resultant error of the on-axis intensity is 12% for IR, 15% for SH, and 18% for UV. The nonlinear coefficients of SPM and XPM with different polarizations were measured, with the results presented in Table 74.III. Both n_2 and γ, which are related through the index of refraction, are presented. Our results for the nonlinear coefficient at 1.053-μm wavelength are in good agreement with the work reported in Refs. 20 and 21, which is shown in the last two columns of Table 74.III. To our knowledge, the nonlinear SPM coefficients at wavelengths of 0.527 μm, and 0.351 μm, and the XPM coefficient between 1.053 μm and 0.527 μm, are the first data set reported for KDP.

In the two-color *Z*-scan, there is a further temporal walk-off between the two colors with different wavelengths in the KDP sample. To measure n_2(*o*-*o*), in which both the probe and the pump beams are ordinary waves, the optical axis of the sample KDP (90° cut) is perpendicular to the polarization of IR and SH pulses. Both the pump and probe beams are *o*-waves in the sample, and the pump pulse (IR) moves 0.51 ps ahead of the probe pulse (SH) after the sample. For measuring n_2(*e*-*e*), both the pump (IR) and probe beams (SH) are *e*-waves in the sample, and the pump pulse moves 0.59 ps ahead of the probe pulse in the sample crystal. We include the walk-off effects in the theoretical fit by dividing the sample into segments and integrating the nonlinear phase experienced in each of the pieces. In each of the segments, the probe beam will experience a different nonlinear phase shift, which is due to the different time delay between the pump and probe; thus, the XPM can be

Table 74.II: The parameters of *Z*-scans for measuring SPM and XPM in KDP and the resultant phase shift Φ_0.

	λ (μm)	Pulse width (ps)	Energy (μJ)	Φ_0
(a)	1.053 (*e*) (SPM)	2.0	91±5	2.3±0.1
(b)	0.527 (*o*) (SPM)	1.41	3.6±0.4	1.8±0.1
(c)	0.351 (*o*) (SPM)	1.45	2.9±0.4	2.1±0.1
(d)	1.053 (*e*), 0.527 (*e*) (XPM) (pump) (probe)	2.0 (IR) 1.41 (SH)	111±7 (IR) <0.2 (SH)	0.51±0.04

Table 74.III: Measured values of n_2 and γ for KDP at 1.053 μm, 0.527 μm, and 0.351 μm for SPM and cross-phase coefficients between 0.527 μm and 1.053 μm. Also shown are results of previous work from Refs. 20 and 21.

	$n_2(10^{-13}$ esu)	$\gamma(10^{-16}$ cm^2/W)	$n_2(10^{-13}$ esu) other work	$\gamma(10^{-16}$ cm^2/W) other work
1.053 μm (*o*)	0.8±0.2	2.3±0.5	0.72[20]	2.9±0.9[21]
(*e*)	0.88±0.2	2.5±0.5	0.78,[20] 1.0±0.3[21]	
0.527 μm (*o*)	1.4±0.4	4.0±1.0		
	1.3±0.3	3.5±0.9		
0.351 μm (*o*)	2.4±0.7	7.0±2.0		
(*e*)	1.2±0.4	3.0±1.0		
0.527 (*e*); 1.053 (*e*) (weak; strong)	0.03±0.01	0.10±0.03		
0.527 (*o*); 1.053 (*o*) (weak; strong)	0.023±0.007	0.06±0.02		

well determined. We could improve the sensitivity of our measurement by putting a predelay crystal[34] before or after the frequency-doubling crystal to compensate for the walk-off introduced in the measured sample.

In conclusion, a top-hat *Z*-scan method was used to measure the phase shift caused by the self- and cross-phase nonlinearity in KDP crystals. The third-order nonlinear coefficient of KDP at different polarizations at wavelengths of 1.053 μm, 0.527 μm, and 0.351 μm was obtained. By considering the temporal walk-off between the pump and probe beams in the crystals, we are also able to estimate the nonlinear index of refraction due to the cross-phase modulation.

ACKNOWLEDGMENT

We thank R. Boni for providing several crystals, R. S. Craxton for performing pulse-width calculations, and both for many helpful discussions. This study was supported by the U.S. Department of Energy Office of Inertial Confinement Fusion under Cooperative Agreement No. DE-FC03-92SF19460, the University of Rochester, and the New York State Energy Research and Development Authority. The support of DOE does not constitute an endorsement by DOE of the views expressed in this article.

REFERENCES

1. W. L. Kruer, *The Physics of Laser Plasma Interactions*, Frontiers in Physics, Vol. 73, edited by D. Pines (Addison-Wesley, Redwood City, CA, 1988), Chap. 5.
2. J. C. Kieffer, P. Audebert, M. Chaker, J. P. Matte, H. Pépin, T. W. Johnston, P. Maine, D. Meyerhofer, J. Delettrez, D. Strickland, P. Bado, and G. Mourou, Phys. Rev. Lett. **62**, 760 (1989).
3. C. Y. Chien, G. Korn, J. S. Coe, J. Squier, G. Mourou, and R. S. Craxton, Opt. Lett. **20**, 353 (1995).
4. R. W. Boyd, *Nonlinear Optics* (Academic Press, Boston, 1992).
5. G. P. Agrawal, *Nonlinear Fiber Optics* (Academic Press, Boston, 1989).
6. K. J. Blow, N. J. Doran, and B. P. Nelson, Opt. Lett. **10**, 393 (1985).
7. M. N. Islam, L. F. Mollenauer, and R. H. Stolen, in *Ultrafast Phenomena V*, edited by G. R. Fleming and A. E. Siegman, Springer Series in Chemical Physics (Springer-Verlag, Berlin, 1986), pp. 46–50.
8. J. D. Kafka and T. Baer, Opt. Lett. **12**, 181 (1987).
9. R. H. Stolen and J. E. Bjorkholm, IEEE J. Quantum Electron. **QE-18**, 1062 (1982).
10. R. R. Alfano *et al.*, Phys. Rev. A **35**, 459 (1987).
11. L. Zheng, R. S. Craxton, and D. D. Meyerhofer, in *Conference on Lasers and Electro-Optics*, Vol. 15, 1995 OSA Technical Digest Series (Optical Society of America, Washington, DC, 1995), pp. 131–132; L. Zheng, "Third-Harmonic Generation of Intense Laser Pulses," Ph.D. thesis, University of Rochester, 1997.
12. M. Sheik-bahae, A. A. Said, and E. W. Van Stryland, Opt. Lett. **14**, 955 (1989).
13. M. Sheik-bahae *et al.*, IEEE J. Quantum Electron. **26**, 760 (1990).
14. S. R. Friberg and P. W. Smith, IEEE J. Quantum Electron. **QE-23**, 2089 (1987).
15. Y.-H. Chuang, Z. W. Li, D. D. Meyerhofer, and A. Schmid, Opt. Lett. **16**, 7 (1991).
16. A. Owyoung, IEEE J. Quantum Electron. **QE-9**, 1064 (1973).
17. M. J. Weber, D. Milam, and W. L. Smith, Opt. Eng. **17**, 463 (1978).
18. M. J. Moran, C.-Y. She, and R. L. Carman, IEEE J. Quantum Electron. **QE-11**, 259 (1975).
19. W. Seka, J. M. Soures, S. D. Jacobs, L. D. Lund, and R. S. Craxton, IEEE J. Quantum Electron. **QE-17**, 1689 (1981).
20. R. Adair, L. L. Chase, and S. A. Payne, Phys. Rev. B **39**, 3337 (1989).
21. D. Milam and M. J. Weber, J. Appl. Phys. **47**, 2497 (1976).
22. M. Sheik-Bahae *et al.*, Opt. Lett. **17**, 258 (1992).
23. R. S. Craxton, IEEE J. Quantum Electron. **QE-17**, 1771 (1981).
24. W. Zhao and P. Palffy-Muhoray, Appl. Phys. Lett. **63**, 1613 (1993).
25. M. Born and E. Wolf, *Principles of Optics: Electromagnetic Theory of Propagation, Interference and Diffraction of Light*, 6th ed. (Pergamon Press, Oxford, 1980), p. 435.
26. J. D. Gaskill, *Linear Systems, Fourier Transforms, and Optics* (Wiley, New York, 1978).
27. Y.-H. Chuang, D. D. Meyerhofer, S. Augst, H. Chen, J. Peatross, and S. Uchida, J. Opt. Soc. Am. B **8**, 1226 (1991).
28. Optical Glass Filters, Scott Glass Technologies, Inc., Duryea, PA 18642.
29. Model GP-MF 702, Panasonic, Secaucus, NJ 07094.
30. PIN 10D 4303, UDT Sensors, Inc., Hawthorne, CA 90250.
31. JD 1000 Joulemeter, Molectron Detector, Inc., Portland, OR 97224.
32. A. E. Siegman, *Lasers* (University Science Books, Mill Valley, CA, 1986).
33. Y. Wang and R. Dragila, Phys. Rev. A **41**, 5645 (1990).
34. Y. Wang, B. Luther-Davis, Y.-H. Chuang, R. S. Craxton, and D. D. Meyerhofer, Opt. Lett. **16**, 1862 (1991).